

# Coaxial Triple-Layered versus Helical $\text{Be}_6\text{B}_{11}^-$ Clusters: Dual Structural Fluxionality and Multifold Aromaticity

Jin-Chang Guo, Lin-Yan Feng, Ying-Jin Wang, Said Jalife, Alejandro Vásquez-Espinal, José Luis Cabellos, Sudip Pan, Gabriel Merino,\* and Hua-Jin Zhai\*

Dedicated to Professor Roald Hoffmann on the occasion of his 80th birthday

**Abstract:** Two low-lying structures are unveiled for the  $\text{Be}_6\text{B}_{11}^-$  nanocluster system that are virtually isoenergetic. The first, triple-layered cluster has a peripheral  $\text{B}_{11}$  ring as central layer, being sandwiched by two  $\text{Be}_3$  rings in a coaxial fashion, albeit with no discernible interlayer Be–Be bonding. The  $\text{B}_{11}$  ring revolves like a flexible chain even at room temperature, gliding freely around the  $\text{Be}_6$  prism. At elevated temperatures (1000 K), the  $\text{Be}_6$  core itself also rotates; that is, two  $\text{Be}_3$  rings undergo relative rotation or twisting with respect to each other. Bonding analyses suggest four-fold ( $\pi$  and  $\sigma$ ) aromaticity, offering a dilute and fluxional electron cloud that lubricates the dynamics. The second, helix-type cluster contains a  $\text{B}_{11}$  helical skeleton encompassing a distorted  $\text{Be}_6$  prism. It is chiral and is the first nanosystem with a boron helix. Molecular dynamics also shows that at high temperature the helix cluster readily converts into the triple-layered one.

**B**oron-based nanoclusters are a fertile ground for unique quasi-planar (2D) structures up to 40 atoms,<sup>[1–6]</sup> extreme coordination environments,<sup>[1]</sup> and intriguing dynamic properties;<sup>[7–17]</sup> all these phenomena are attributed to the electron deficiency of boron. During the past decades, nanomachines (including molecular rotors)<sup>[18]</sup> have emerged as a hot topic in chemistry and nanoscience. A spectroscopic study of Zhai, Wang, and Boldyrev in 2010 on a 2D wheel-like  $\text{B}_{19}^-$  cluster<sup>[4]</sup> sparked an immediate proposal of molecular Wankel motor by Merino, Heine, and co-workers,<sup>[7]</sup> which was subsequently extended to a series of circular clusters:  $\text{B}_{13}^+$ ,  $\text{B}_{18}^{2-}$ ,  $\text{B}_{20}^{2-}$ , and  $\text{B}_{12}\text{Ir}^-$ .<sup>[8–14]</sup> Elongated boron clusters ( $\text{B}_{11}$ ,  $\text{B}_{11}^-$ , and  $\text{B}_{15}^+$ )

were lately shown as well to be fluxional, behaving like subnanoscale tank treads.<sup>[15,16]</sup> Quite recently, all the predictions have made sense in view of the observation of fluxionality of  $\text{B}_{13}^+$  via cryogenic ion vibrational spectroscopy.<sup>[17]</sup> Questions remain open as to whether the molecular rotor goes three-dimensional (3D); or even better, whether multiple rings and multifold fluxionality coexist in a nano-system; and if yes, what governs such unconventional dynamics.

Boron clusters adopt a variety of topologies including 2D clusters<sup>[1–6]</sup> and borospherenes.<sup>[6]</sup> However, multiple-layered forms or helical ones have not been reported. To “design” such clusters, we chose to explore the combination between boron and beryllium. A prior work by Molina et al.<sup>[19]</sup> suggested that the  $\text{Be}_6\text{B}_{12}$  cluster holds a  $\text{Be}_6$  octahedron encircled inside a  $\text{B}_{12}$  ring. One can expect that in a Be–B binary cluster, the Be atoms tend to be loosely bound with each other and have a potency to donate electrons, creating a frame for new boron topologies. Such donation balances the electron deficiency of boron and strengthens the Be–Be interactions.<sup>[20]</sup> By tuning the size of B ring, number of Be atoms, charge state, and electron counting, and with trial and error, we eventually reach a  $\text{Be}_6\text{B}_{11}^-$  cluster, the two lowest-energy isomers of which are nearly isoenergetic and yet show distinct topologies: A helix-type  $C_2$  cluster versus a coaxial multiple-layered  $C_{2v}$  cluster, the latter possessing fantastic dynamic properties. The structures represent the first boron helix, as well as the first 3D Wankel motor with dual dynamic modes.

The potential energy surface of  $\text{Be}_6\text{B}_{11}^-$  was systematically explored using the coalescence kick (CK) method,<sup>[21,22]</sup> with 8000 stationary points being probed (both singlet and triplet states). Further exploration was carried out using the Cuckoo search algorithm as implemented in the Bilatu code.<sup>[23,24]</sup> Low-lying isomers were subsequently reoptimized at the PBE0-D3/def2-TZVP level, in which dispersion is included in the functional. The low-energy structures (**1–20**) are collected in the Supporting Information, Figure S1. Relative energies of top isomers were benchmarked at single-point CCSD(T)/def2-TZVP//PBE0-D3/def2-TZVP level.<sup>[25]</sup> At CCSD(T), two competitive structures **1** and **2** were found within 0.4 kcal mol<sup>-1</sup> (including corrections for zero-point energy (ZPE) at PBE0-D3; Figure 1), which are reasonably well separated from alternative isomers. Cluster **1** ( $C_2$ , <sup>1</sup>A) has a boron helix screwing into a distorted  $\text{Be}_6$  framework, the Cartesian coordinates of which are shown in

[\*] Dr. J.-C. Guo  
Institute of Materials Science & Department of Chemistry  
Xinzhou Teachers University  
Xinzhou 034000, Shanxi (China)

Dr. J.-C. Guo, L.-Y. Feng, Y.-J. Wang, Prof. Dr. H.-J. Zhai  
Nanocluster Laboratory, Institute of Molecular Science  
Shanxi University, Taiyuan 030006 (China)  
E-mail: hj.zhai@sxu.edu.cn

S. Jalife, A. Vásquez-Espinal, J. L. Cabellos, S. Pan, Prof. Dr. G. Merino  
Departamento de Física Aplicada, Centro de Investigación y de  
Estudios Avanzados, Unidad Mérida  
km 6 Antigua carretera a Progreso, Apdo. Postal 73, Cordemex,  
97310, Mérida, Yuc. (México)  
E-mail: gmerino@cinvestav.mx

Supporting information and the ORCID identification number(s) for the author(s) of this article can be found under:  
<https://doi.org/10.1002/anie.201703979>.

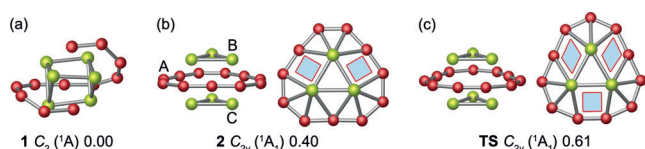


**Figure 1.** Optimized structures of a) cluster **1** and b) top- and side-views of cluster **2** at PBE0-D3/def2-TZVP level. Shown in c) is the transition state (TS<sub>rev</sub>) in **2** associated to revolution of peripheral B<sub>11</sub> ring around Be<sub>6</sub> prism. Relative energies (including barrier for revolution) are indicated in kcal mol<sup>-1</sup> at CCSD(T)/def2-TZVP//PBE0-D3/def2-TZVP, with corrections for zero-point energy (ZPE) at PBE0-D3. Note that two Be<sub>3</sub> layers within Be<sub>6</sub> prism in **2** can also rotate with respect to each other.

Table S1 along with other selected species. It is chiral, and its enantiomer (not shown) is readily constructed and confirmed. Cluster **2** ( $C_{2v}$ ,  $^1A_1$ ) has a triple-layered geometry, which consists of three rings (Be<sub>3</sub>, B<sub>11</sub>, and Be<sub>3</sub>) being coaxially piled up. Among higher-energy isomers is circular **5** ( $C_2$ ,  $^1A$ ), situating at 5.20 kcal mol<sup>-1</sup> above **2**. Structures **2** and **5** differ by a twist of the Be<sub>3</sub> ring at bottom by 60°; the former has an eclipsed conformation and the latter a staggered one.

In species **1** and **2**, the B–B distances range from 1.51 to 1.59 Å (Supporting Information, Figure S2), being markedly shorter than a B–B single bond and similar to those in free B<sub>8</sub> and B<sub>9</sub><sup>-</sup> molecular wheels.<sup>[1]</sup> Computed Wiberg bond index (WBI) is 1.29–1.62 for B–B bonds. In contrast, the Be<sub>6</sub> core in **1** and **2** show geometric differences. In **1**, the Be<sub>6</sub> fragment adopts an irregular shape with Be–Be distances of 2.16 to 2.46 Å; whereas in **2**, the beryllium core is a triangular prism with Be–Be distances of 2.19–2.25 Å in the triangles, which are shorter than that in Be<sub>2</sub> dimer (2.444 Å).<sup>[26]</sup> The interlayer Be–Be distances in **2** are even shorter (2.10–2.17 Å), although no direct bonding exists between the Be<sub>3</sub> rings, which is supported by interlayer Be–Be WBI values of 0.07–0.08. This shortening appears to be due to electrostatic effects. Indeed, the natural charges from natural population analysis (NPA)<sup>[27]</sup> reveal a substantial charge transfer from the Be fragment to the B skeleton. Boron fragments in **1** and **2** bear a charge of –5.84 and –4.62 |e|, respectively (Supporting Information, Figure S3), the formal charge states of which are significantly higher (see below). These values indicate a higher intramolecular electron donation in **1** than in **2**. In short, the Be<sub>6</sub> core serves as an electron reservoir, capable of donating vast amount of charges depending on the topology of boron.

How do clusters **1** and **2** behave dynamically? Born–Oppenheimer molecular dynamics (BOMD) simulations<sup>[28]</sup> offer a straightforward answer. Three short movies extracted from the BOMD simulations at different temperatures are presented in the Supporting Information. At low temperatures only slight structural modifications are perceived in **1**. However, at 1200 K, **1** transforms to **2** within several steps. In contrast, BOMD indicates that **2** moves dynamically in both revolution and rotation modes, vividly mimicking the earth–moon system. At 300 K (and beyond), the outer B<sub>11</sub> ring in **2** revolves (or orbits) freely around the Be<sub>6</sub> core, behaving like a spinning hula hoop. All B atoms move in plane in a concerted manner and the B ring shows remarkable flexibility, akin to a continuous track. The Be<sub>6</sub> unit adjusts instantaneously according to the need of B ring so that it

always fits perfectly in the latter. The two Be<sub>3</sub> rings move largely in phase at low temperature of 300 K. While revolution proceeds in random directions, either clockwise or anticlockwise, the B ring still accomplishes two-thirds of a loop in 25 ps at 300 K. Considering the absolute velocity, we estimate a full turn of revolution in approximate 20 ps. At elevated temperatures, the revolution of B ring is retained. However, a second mode of dynamics emerges. The Be<sub>6</sub> core now rotates on its own. To be precise, two Be<sub>3</sub> rings become somewhat separable at 600 K and they eventually rotate (or twist) with respect to each other at 1000 K, albeit at a much lower speed than revolution. Revolution and rotation are coaxial, with the axis linking the centers of three rings.

Energy pathways for revolution and rotation in cluster **2** are illustrated in Figure 2. Starting from **2**, the revolution (lower pathway) takes place via a transition state (denoted as TS<sub>rev</sub>) and returns to **2**. For the rotation, isomer **5** (Supporting Information, Figure S1) is an intermediate state and a full step of rotation is accomplished via two identical TS structures (denoted as TS<sub>rot</sub>; upper pathway). The barriers for revolution and rotation are 0.15 and 4.52 kcal mol<sup>-1</sup>, respectively, at PBE0-D3 level (further refined to 0.21 and 4.70 kcal mol<sup>-1</sup> at single-point CCSD(T)), which differ by one order of magnitude, consistent with the fact that the latter mode is in play only at high temperature (1000 K). The lowest vibrational mode of **2** (45 cm<sup>-1</sup>; Supporting Information, Figure S4a) is related to revolution, which leads to square-to-rhombus distortion of the shaded “defective” areas in Figure 1b, transforming **2** into TS<sub>rev</sub> and vice versa. A similar imaginary soft mode (50i cm<sup>-1</sup>) is present in TS<sub>rev</sub>. For both modes, two Be<sub>3</sub> rings move completely in phase; that is, as a collective Be<sub>6</sub> prism. In contrast, the rotation (twisting) involves modes of 87 and 426 cm<sup>-1</sup> (Supporting Information, Figure S4b), in which two Be<sub>3</sub> rings move in opposite directions. The higher mode appears to determine the overall rotational barrier (upper curve; Figure 2).

To understand the structural and dynamic properties of clusters **1** and **2**, it is essential to perform chemical bonding analyses. An overall bonding picture can be obtained from adaptive natural density partitioning (AdNDP),<sup>[29]</sup> which is an extension of natural bond orbital (NBO) analysis. It repre-

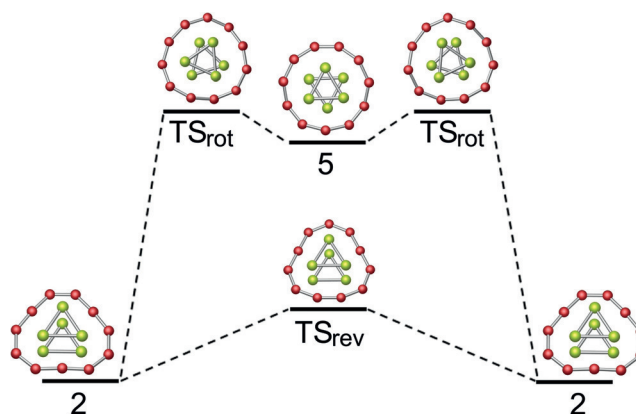


**Figure 2.** Energy pathways for revolution (lower curve) and rotation (upper curve) of cluster **2**. The former movement proceeds via TS<sub>rev</sub> whereas the latter takes places via local minimum **5** and two identical TS<sub>rot</sub> structures. See text for relative energies and energy barriers.

sents the electronic structure of a molecular system in terms of  $n$ -center two-electron ( $nc$ - $2e$ ) bonds, with  $n$  ranging from one to the total number of atoms in the molecule. Thus, AdNDP recovers the Lewis elements (lone pairs and  $2c$ - $2e$  bonds), as well as the delocalized  $nc$ - $2e$  bonds. The major difference between **1** and **2** is the presence of one extra B–B bond in **2**. As shown in Figures 3 and 4, out of 46 electrons (23 pairs) in  $\text{Be}_6\text{B}_{11}^-$ , ten and eleven  $2c$ - $2e$   $\sigma$  bonds are present in **1** and **2**, respectively. All other bonds are delocalized. There are two  $4c$ - $2e$   $\sigma$  bonds in **1** involving the B tip and three Be atoms, four  $\pi$  bonds, and seven delocalized  $\sigma$  bonds.

For cluster **2**, each  $\text{Be}_3$  ring is held together by a  $3c$ - $2e$   $\sigma$  bond (Figure 4a; top row), whereas peripheral  $\text{B}_{11}$  ring possesses ten delocalized  $\sigma$  (middle row) and  $\pi$  (bottom row) electrons. Its canonical molecular orbitals (CMOs) give the

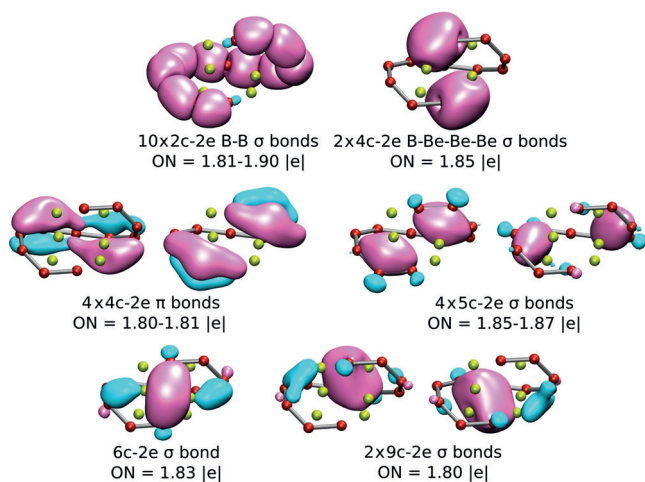


**Figure 3.** AdNDP bonding pattern of cluster **1**. Occupation numbers (ONs) are shown.

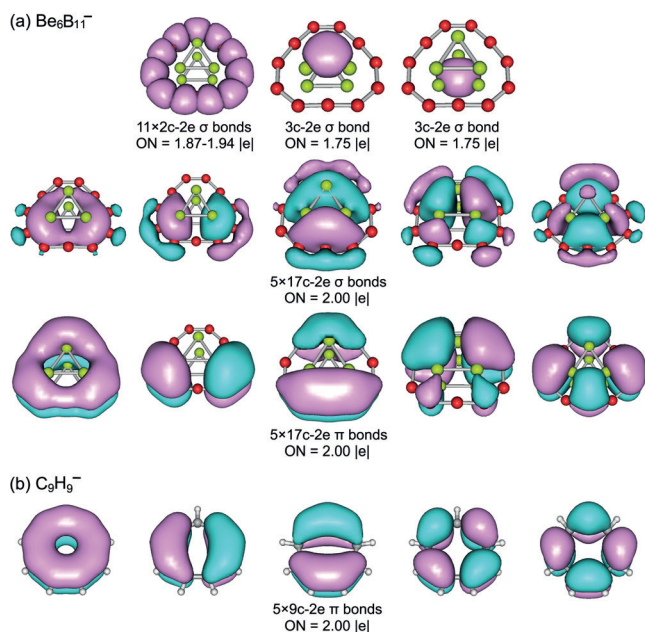


**Figure 4.** AdNDP bonding pattern of a) cluster **2** as compared to that of b)  $\text{C}_9\text{H}_9^-$ . Occupation numbers (ONs) are shown.

same picture; see the Supporting Information, Figures S5 and S6 for details. Note that the  $10\sigma$  ( $\text{B}_{11}$ ),  $10\pi$  ( $\text{B}_{11}$ ), and two  $2\sigma$  ( $\text{Be}_3$ ) subsystems are essentially delocalized and cannot be transformed to Lewis elements, rendering four-fold  $\pi$  and  $\sigma$  aromaticity for **2**,<sup>[30]</sup> which is unprecedented in a molecular system. Note that the  $10\sigma/10\pi/2\sigma/2\sigma$  electron countings all conform to the  $(4n+2)$  Hückel rule. With the above analyses, it is clear that cluster **2** can be formally formulated as  $[\text{Be}_3]^{4+}[\text{B}_{11}]^{9-}[\text{Be}_3]^{4+}$ . Since the shorter Be–Be distances in cluster **1** are comparable to those in **2**, the formal charge state of  $\text{B}_{11}$  helix in **1** is probably  $[\text{B}_{11}]^{9-}$  or even higher due to the larger amount of charge transfers (Supporting Information, Figure S3). Thus, clusters **1** and **2** hint the possibilities to stabilize highly charged monocyclic or helical boron fragments using beryllium as counterions.

According to AdNDP, the  $\pi$  system in cluster **2** is similar to that in cyclononatetraenyl anion ( $\text{C}_9\text{H}_9^-$ ; Figure 4b). Their corresponding CMOs are compared in the Supporting Information, Figure S7, showing one-to-one correspondence. Nucleus independent chemical shifts (NICS)<sup>[31]</sup> were calculated for **2**,  $\text{C}_9\text{H}_9^-$ , and  $\text{C}_6\text{H}_6$ , which are highly negative (Supporting Information, Table S2), in line with multifold aromaticity for **2**. The CMOs and AdNDP pattern in  $\text{TS}_{\text{rev}}$  structure (Supporting Information, Figures S8 and S9) are similar to those in **2**, except for a flow of electron clouds.

Given the tiny energy difference, both clusters **1** and **2** are anticipated to be observed in the gas-phase experiments. Cluster **1** is the first boron helix, whose skeleton can be associated to its large intramolecular electron transfer. On the other hand, the vastly rich, four-fold aromaticity in cluster **2** underlies its dynamics. In such a highly delocalized triple-layered system, an individual B–Be or Be–Be bond does not exist. The  $\text{Be}_3/\text{B}_{11}/\text{Be}_3$  rings in **2** are thus independent and isolated structural blocks, being lubricated via dilute, delocalized, fluxional electron clouds. This bonding situation makes the revolution or orbiting of  $\text{B}_{11}$  ring nearly barrierless. The “mysterious” interconnection between two  $\text{Be}_3$  rings lies in HOMO–4 and HOMO–5 (Supporting Information, Figure S5), which couple the  $\text{Be}_3$  rings as a  $\text{Be}_6$  prism. However, the interlayer Be–Be bonding is rather weak, allowing activation of the rotational (twisting) mode at elevated temperatures. Dual dynamic modes are unknown in the literature for any nanosystem. With both revolution and rotation dynamics, cluster **2** shall serve as an ultimate nanoobject that mimics the earth–moon system, yet shrinking the latter in size by 18 orders of magnitude.<sup>[32]</sup>

## Methods Section

Structural searches of  $\text{Be}_6\text{B}_{11}^-$  were performed using the CK<sup>[21,22]</sup> and Bilatu<sup>[23,24]</sup> programs, in combination with manual structural constructions. Over 8000 stationary points (for singlet and triplet states) were probed at the PBE0/LanL2DZ level. Candidate low-lying isomers were further optimized using the PBE0-D3 method with def2-TZVP basis set. Vibrational frequencies were analyzed at the same level to confirm them as true minima and to get zero-point energy (ZPE) corrections. To benchmark the energetics, single-point CCSD(T) calculations were carried out using the optimized PBE0-D3/def2-TZVP geometry. QST3 and intrinsic reaction coordinate (IRC) calculations were performed at PBE0-D3 to search and

confirm TS structures. NBO and CMO analyses were carried out at PBE0-D3, the former using the NBO 3.1 program. AdNDP calculations were done at PBE0. Charge density differences, orbital composition, and AdNDP analyses were performed using Multiwfn<sup>[33]</sup> and all other calculations using Gaussian 09 package.<sup>[34]</sup> BOMD simulations were carried out at PBE0/DZVP-GTH level, using the CP2K package. Molecular structures, CMOs, and AdNDP results were visualized using CYLview<sup>[35]</sup> and Molekel 5.4.<sup>[36]</sup>

## Acknowledgements

This work was supported by the National Natural Science Foundation of China (21573138), the Scientific and Technological Innovation Programs of Higher Education Institutions in Shanxi (2017170), and the Sanjin Scholar Distinguished Professors Program. Work done in Mexico was supported by Conacyt (Grant CB-2015-252356). CGSTIC (Xihucuoal) and ABACUS at Cinvestav are acknowledged for allocation of computational resources. S.J. thanks Conacyt for the PhD fellowship. S.P. and A.V.-E. thank Conacyt for the Postdoc fellowships.

## Conflict of interest

The authors declare no conflict of interest.

**Keywords:** boron clusters · boron helix · coaxial triple-layered cluster · multifold ( $\pi$  and  $\sigma$ ) aromaticity · structural fluxionality

**How to cite:** *Angew. Chem. Int. Ed.* **2017**, *56*, 10174–10177  
*Angew. Chem.* **2017**, *129*, 10308–10311

- [1] H. J. Zhai, A. N. Alexandrova, K. A. Birch, A. I. Boldyrev, L. S. Wang, *Angew. Chem. Int. Ed.* **2003**, *42*, 6004–6008; *Angew. Chem.* **2003**, *115*, 6186–6190.
- [2] H. J. Zhai, B. Kiran, J. Li, L. S. Wang, *Nat. Mater.* **2003**, *2*, 827–833.
- [3] D. Y. Zubarev, A. I. Boldyrev, *J. Comput. Chem.* **2007**, *28*, 251–268.
- [4] W. Huang, A. P. Sergeeva, H. J. Zhai, B. B. Averkiev, L. S. Wang, A. I. Boldyrev, *Nat. Chem.* **2010**, *2*, 202–206.
- [5] W. L. Li, Y. F. Zhao, H. S. Hu, J. Li, L. S. Wang, *Angew. Chem. Int. Ed.* **2014**, *53*, 5540–5545; *Angew. Chem.* **2014**, *126*, 5646–5651.
- [6] H. J. Zhai, Y. F. Zhao, W. L. Li, Q. Chen, H. Bai, H. S. Hu, Z. A. Piazza, W. J. Tian, H. G. Lu, Y. B. Wu, Y. W. Mu, G. F. Wei, Z. P. Liu, J. Li, S. D. Li, L. S. Wang, *Nat. Chem.* **2014**, *6*, 727–731.
- [7] J. O. C. Jiménez-Halla, R. Islas, T. Heine, G. Merino, *Angew. Chem. Int. Ed.* **2010**, *49*, 5668–5671; *Angew. Chem.* **2010**, *122*, 5803–5806.
- [8] G. Martínez-Guajardo, A. P. Sergeeva, A. I. Boldyrev, T. Heine, J. M. Ugalde, G. Merino, *Chem. Commun.* **2011**, *47*, 6242–6244.
- [9] D. Moreno, S. Pan, L. L. Zeonjuk, R. Islas, E. Osorio, G. Martínez-Guajardo, P. K. Chattaraj, T. Heine, G. Merino, *Chem. Commun.* **2014**, *50*, 8140–8143.
- [10] F. Cervantes-Navarro, G. Martínez-Guajardo, E. Osorio, D. Moreno, W. Tiznado, R. Islas, K. J. Donald, G. Merino, *Chem. Commun.* **2014**, *50*, 10680–10682.
- [11] I. A. Popov, W. L. Li, Z. A. Piazza, A. I. Boldyrev, L. S. Wang, *J. Phys. Chem. A* **2014**, *118*, 8098–8105.
- [12] L. Liu, D. Moreno, E. Osorio, A. C. Castro, S. Pan, P. K. Chattaraj, T. Heine, G. Merino, *RSC Adv.* **2016**, *6*, 27177–27182.
- [13] T. B. Tai, A. Ceulemans, M. T. Nguyen, *Chem. Eur. J.* **2012**, *18*, 4510–4512.
- [14] S. Jalife, L. Liu, S. Pan, J. L. Cabellos, E. Osorio, C. Lu, T. Heine, K. J. Donald, G. Merino, *Nanoscale* **2016**, *8*, 17639–17644.
- [15] Y. J. Wang, X. Y. Zhao, Q. Chen, H. J. Zhai, S. D. Li, *Nanoscale* **2015**, *7*, 16054–16060.
- [16] Y. J. Wang, X. R. You, Q. Chen, L. Y. Feng, K. Wang, T. Ou, X. Y. Zhao, H. J. Zhai, S. D. Li, *Phys. Chem. Chem. Phys.* **2016**, *18*, 15774–15782.
- [17] M. R. Fagiani, X. Song, P. Petkov, S. Debnath, S. Gewinner, W. Schöllkopf, T. Heine, A. Fielicke, K. R. Asmis, *Angew. Chem. Int. Ed.* **2017**, *56*, 501–504; *Angew. Chem.* **2017**, *129*, 515–519.
- [18] G. S. Kottas, L. I. Clarke, D. Horinek, J. Michl, *Chem. Rev.* **2005**, *105*, 1281–1376.
- [19] L. M. Molina, M. J. López, I. Cabria, J. A. Alonso, N. H. March, *Phys. Rev. B* **2005**, *72*, 113414.
- [20] For example, the neutral Be<sub>3</sub> cluster is sort of a van der Waals system, because canonical molecular orbitals (CMOs) of bonding/nonbonding/antibonding types are fully occupied, canceling each other and resulting in negligible net bonding. For a positively charged Be cluster, the antibonding components are less occupied, leading to enhanced bonding with respect to neutral.
- [21] A. P. Sergeeva, B. B. Averkiev, H. J. Zhai, A. I. Boldyrev, L. S. Wang, *J. Chem. Phys.* **2011**, *134*, 224304.
- [22] M. Saunders, *J. Comput. Chem.* **2004**, *25*, 621–626.
- [23] R. Grande-Aztatzi, P. R. Martínez-Alanis, J. L. Cabellos, E. Osorio, A. Martínez, G. Merino, *J. Comput. Chem.* **2014**, *35*, 2288–2296.
- [24] A. Ramirez-Manzanares, J. Pena, J. M. Azpiroz, G. Merino, *J. Comput. Chem.* **2015**, *36*, 1456–1466.
- [25] K. Raghavachari, G. W. Trucks, J. A. Pople, M. Head-Gordon, *Chem. Phys. Lett.* **1989**, *157*, 479–483.
- [26] A. Kalemios, *J. Chem. Phys.* **2016**, *145*, 214302.
- [27] A. E. Reed, L. A. Curtis, F. A. Weinhold, *Chem. Rev.* **1988**, *88*, 899–926.
- [28] J. VandeVondele, M. Krack, F. Mohamed, M. Parrinello, T. Chassaing, J. Hutter, *Comput. Phys. Commun.* **2005**, *167*, 103–128.
- [29] D. Y. Zubarev, A. I. Boldyrev, *Phys. Chem. Chem. Phys.* **2008**, *10*, 5207–5217.
- [30] Intriguingly, the in-phase and out-of-phase  $\sigma$  couplings between the Be<sub>3</sub>/Be<sub>3</sub> rings in **2** (HOMO–5/HOMO–15 versus HOMO–4/HOMO–13; Supporting Information, Figure S6) allow the Be 2s electrons to participate in both  $\sigma$  and  $\pi$  bonding with the B<sub>11</sub> ring. For the  $\pi$  framework, two layers of Be<sub>3</sub> 2s clouds manage to couple out-of-phase, disguised as a “ $\pi$ ” component.
- [31] P. v. R. Schleyer, C. Maerker, A. Dransfeld, H. J. Jiao, N. J. R. van Eikema Hommes, *J. Am. Chem. Soc.* **1996**, *118*, 6317–6318.
- [32] The earth is  $1.27 \times 10^7$  m in size and the orbit of the moon has a diameter of  $7.6 \times 10^8$  m. For cluster **2**, the size of Be<sub>6</sub> prism core has a height of  $2.2 \times 10^{-10}$  m and the diameter of B<sub>11</sub> ring is  $5.38 \times 10^{-10}$  m.
- [33] T. Lu, F. W. Chen, *J. Comput. Chem.* **2012**, *33*, 580–592.
- [34] Gaussian09 (Revision D.01), M. J. Frisch, et al., Gaussian, Inc., Wallingford, Connecticut, **2009**.
- [35] CYLview, 1.0b, C. Y. Legault, Université de Sherbrooke, **2009** (<http://www.cylview.org>).
- [36] Molekel, version 5.4.0.8, U. Varetto, Swiss National Supercomputing Centre, Manno, Switzerland, **2009**.

Manuscript received: April 17, 2017

Accepted manuscript online: July 7, 2017

Version of record online: July 24, 2017